Nickel–molybdenum catalyst for combined steam/dry reforming

Majewski, Artur; singh, sunit Kumar; Labhasetwar, Nitin; Steinberger-Wilckens, Robert

A0809

Nickel–molybdenum catalyst for combined steam/dry reforming

Artur J Majewski (1), Sunit Kumar Singh (2), Nitin K Labhasetwar (2), Robert Steinberger-Wilckens (1)
(1) School of Chemical Engineering, University of Birmingham,
Edgbaston, B15 2TT, UK
(2) Energy and Resource Management Division, CSIR-National Environmental Engineering Research Institute (NEERI),
Nehru Marg, Nagpur - 440 020, India
a.j.majewski@bham.ac.uk

Abstract

A series of supported Ni-Mo catalysts were synthesised through a deposition-co-precipitation method (DcP) and investigated in combined dry and steam reforming of biogas. The morphology of the oxide precursors and reduced catalysts and their composition were determined via XRF, TEM, SEM, TGA, TPR, BET, and XRD. Modifications to Ni:Mo loading changed the catalyst reduction behaviour and the types of phases formed. The results obtained revealed that the nickel-molybdenum oxide precursors consisted of a nickel molybdate phase. The prepared Ni-Mo catalysts supported by YSZ, GDC and CSZ with improved carbon tolerance have the potential to be used as anodes in SOFC. Those catalysts were compared to conventional catalysts with Al_2O_3 and TiO_2 supports typical for reforming catalysts.

Introduction

Hydrogen produced from biogas is one option to supply 'green' zero-carbon hydrogen from renewable sources. Efficient hydrogen production by biogas reforming requires using a catalyst to minimise the kinetic barriers imposed by the activation energy for the formation of reaction intermediates on the catalyst surface. Most common catalysts used for reforming reactions and hydrogen production are based on Ni owing to its high activity and low cost. Reforming catalysts are traditionally composed of Ni supported on porous support materials.

Adjusting reforming conditions and the application of highly active reforming catalysts is a cost-effective method to solve issues with combined steam and dry reforming. The presence of molybdenum in the Ni-based catalyst can influence catalyst selectivity and efficiency toward a number of reactions [1]. A combination of those two metals is supposed to result in an enhanced catalyst activity [2]. Ni-Mo catalysts are applied for hydrotreating reactions in petroleum refining processes and especially in the removal of sulphur [3]. The Mo-rich catalyst can be effective in hydrodesulphurisation [4]. Amorphous Ni-Mo nanopowders synthesised by reduction of Ni-Mo oxides have much-improved activity in comparison to pure Ni catalysts [5]. For the Ni-Mo bimetallic catalysts, two solid solutions can be formed: one being Ni-rich and the other Mo-rich. The increase in Ni-rich phase enhances the catalyst's activity and the presence of the Mo phase stabilises the catalyst [1, 6]. The addition of Mo in a catalyst can improve performance for S-containing biogas due to the formation of a NiMoS phase [4].

The hydrodesulphurisation properties of those catalysts can find application in biogas reforming that might be an attractive option for solid oxide fuel cells (SOFCs). SOFCs are highly efficient energy converters for hydrogen and hydrocarbon fuels. Potential coke formation when operating on hydrocarbons still calls for research on novel carbon tolerant anodes. Ma et al. [7] observed that for high metal loading (Ni:Mo ratio) on Ni-Mo catalysts in SOFC anodes catalyst deactivation resulted during steam reforming due to Ni sintering and coke deposition. Although aqueous impregnation methods with additional nano-scale catalysts [8, 9] showed to be effective in coke deposition reduction, but they still need verification to confirm long-term stability due to the common tendency of nanosized particles to agglomerate at high-temperatures. An alternative is the introduction of dispersed nanoparticles during anode preparation, for example, by a deposition-precipitation method.

Deposition-precipitation has many advantages for catalyst synthesis such as strong metal-support interaction, increased surface area and possibility to increase the amount of metal loading [10]. Additionally, the introduction of carbon to transition metal lattices by the formation of carbides (like Mo_2C) may affect the electronic negativity and improve the desired catalytic properties [11]. Bulk molybdenum carbide itself is catalytically active in hydrogen production reactions but supported metal/Mo carbides show higher catalytic activity [11]. Pure Mo_2C is not active in dry reforming [12]. Introduction of Mo-carbide to the anode structure can improve stability owing to a high melting point and by mitigating atom mobility at elevated temperatures owing to an increase in lattice distortion [6]. It was reported [13] that supported Mo_2C catalysts are much more active than the unsupported structure. Therefore, there is scope for further improvement in the performance of Ni-Mo supported catalysts by manipulating their aggregation, for example, by using a variety of supports.

1. Scientific Approach

This study focuses on the synthesis of supported Ni-Mo catalysts and the analysis of the effect of support and molybdenum addition on the catalyst morphology and performances in biogas reforming. In this report, we demonstrate the fabrication of nickel-molybdenum nanoparticle arrays on a range of supports. To explore whether such compounds are effective as biogas reforming catalysts, a series of nickel-molybdenum samples were synthesised by deposition-co-precipitation and evaluated in reforming reactions. The proposed approach allows development of high dispersion of the catalyst on the support surface. Attention is given to the effect of Mo_2C formation on catalyst activity and influence of support and Ni:Mo molar proportions on the catalytic performance.

2. Experiments

The thermogravimetric analysis (TGA) of temperature-dependent mass change profiles was performed using a thermogravimetric analyser Netzsch 209F1. The sample mass was 10 to 20 mg. The heating rate was $5^oC\ min^{-1}$ in a $5\%H_2/N_2$ flow at flow rate 35 ml min^{-1}, carried out between room temperature and 1,000°C.
The BET surface area was determined by N_2 adsorption-desorption isotherms on a Micromeritics TriStar II Plus. Samples were degassed at 200°C before the experiment was performed.
The structure of the catalyst was analysed by X-ray powder diffraction (XRD) using a Bruker D8 Advance. Analyses were carried out at room temperature in the 2Θ range from 20 to 70°. Scanning speed was $2.2^o \cdot min^{-1}$ for all samples.
The chemical composition of the catalyst was investigated using X-ray fluorescence spectrometry (XRF) on a Bruker S8 Tiger. For analysis, 0.5 g of each sample was ground and placed in 8 mm sample cups with a 2 µm Mylar thin film.
The morphological properties of the tested catalysts and supports were measured using a Scanning Electron Microscope (SEM) Philips Xl-30; accelerating voltage was 15-20 kV.
Particle morphology was examined by transmission electron microscopy (TEM). Samples of the catalyst were suspended in ethanol by sonication. A carbon film on a copper microgrid was used as a sample holder and examined with the JEOL TEM-2100.

Preparation of nickel-molybdenum catalysts
The supported binary Ni-Mo catalysts were synthesised using a deposition-co-precipitation procedure on commercial support powders with urea as a reducing agent. Aqueous solutions of the Ni and Mo precursors i.e. $Ni(NO_3)_2 \cdot 6H_2O$) and $(NH_4)_6Mo_7O_{24} \cdot 4H_2O$ respectively (both Aldrich) were mixed with a support. All selected supports (**YSZ** - TOSOH corporation; 8 mole% Y; **GDC** - Fuel Cell Materials; 10 mole% Gd; **Al_2O_3** - Polymer Innovations Inc; **TiO_2** - Sigma-Aldrich; **CSZ** - United Ceramics Limited 14 mole% Ce) were pre-treated at 800°C (air, 5 h) to eradicate impurities. The pre-treatment affected the support structure reducing the surface area (especially with GDC). The Ni-Mo was deposited on 5 support materials: YSZ, Al_2O_3, TiO_2, DGC and CSZ. The porosity of the selected support materials was relatively low for reforming catalyst application. However, porosity in SOFC anodes is further introduced by subsequent reduction and by addition of sacrificial pore forming agents.
According to the literature [11], Ni-Mo-C structures are dense with a low specific surface area. Additionally, Hirose et al. [14] reported that with the increase in temperature of catalyst treatment during fabrication the surface area of the Ni-Mo bulk decreases.

Therefore, it is important to select a support material and deposition technique that allows high dispersion of the active phase on the support surface with nano-sized particles. The selected deposition-co-precipitation method resulted in the formation of more stable Ni-Mo catalyst structures than mechanical mixing (a common method in SOFC anode formation) [12].

Ni-Mo nitrate solution taken during catalyst preparation had a molar proportion of Ni:Mo 2.3:1 for catalysts 1 to 5 and 9 (Ni-Mo precipitate), Ni:Mo 3.4:1 for catalysts 6, Ni:Mo 4.7:1 for catalyst 7 and for catalyst 8, the Ni:Mo molar ratio was 0.3:1 (Table 1). Urea (Aldrich CN_2H_4O) was added to the Ni-Mo suspension after heating to 95°C and held for 4 h at 95°C to allow deposition-co-precipitation leading to precipitation of a green mixed Ni−Mo oxide. The step was repeated to obtain 10 to 15wt% metallic loading of the active metal. After washing with water to eliminate anions and remaining cations, samples of catalysts were dried and calcined at 800°C in air for 5 h. This step was followed by 1 h heat-treatment (temperature-programmed reduction) to reduce the metal oxides at 750°C (under an atmosphere of H_2:CH_4:N_2 molar ratio 50:25:25) with a 10°C min^{-1} heating rate (N_2 during heating). This completed the metal precursor reduction and eliminated their ligands. The catalyst reduction combined with carburisation is a complex process. During that step (solid-gas reaction), H_2 acts as the reduction agent for the deposited Ni and Mo oxides, while CH_4 is the carbon source for carbide formation (deposited in the same step). Selected support materials YSZ, GDC and CSZ are typical for the SOFC application. Using those materials as a support for the reforming catalyst opens up the possibility to develop highly active and coke resistant SOFC anodes.

Characterisation of the nickel-molybdenum catalyst

After calcination, the tested support materials had a relatively low surface area >10 m^2g^{-1}. Typical reforming catalyst supports Al_2O_3 and TiO_2, which were selected for comparison to SOFC materials, had a surface area similar to YSZ. Coating by Ni-Mo slightly increased the surface area for YSZ, Al_2O_3, and CSZ supports (catalysts after reduction). The addition of a metal phase at the surface of substrates created heterogeneity and increased roughness owing to the deposition of nanoparticles, thereby increasing the surface area. However, the surface area for TiO_2 and GDC catalyst precursors slightly decreased after the metal loading. This suggests that Ni-Mo co-deposition blocked some pores and dispersion of deposited particles was lower.

Table 1. Structural parameters of the synthesised Ni-Mo catalysts (after reduction).

No	Catalyst	XRF [%]		BET [m^2g^{-1}]
		Ni	Mo	
1	13Ni-7Mo/YSZ	13.7	7.6	7.4
2	13Ni-7Mo/GDC	13.1	6.2	9.2
3	13Ni-7Mo/Al_2O_3	12.5	7.8	10.4
4	13Ni-7Mo/TiO_2	12.1	6.8	9.3
5	13Ni-7Mo/CSZ	12.3	6.6	5.4
6	23Ni-7Mo/YSZ	22.7	6.3	7.1
7	13Ni-3.5Mo/YSZ	13.5	3.5	6.2
8	13Ni-16Mo/YSZ	12.2	15.4	5.8
9	13Ni-7Mo precipitate	65.1*	34.4*	--

*dried overnight at 105°C (not calcined, not reduced).

According to XRF analyses (oxygen not included), the loading of Ni and Mo was close to the nominal. Increasing Ni content from 13% to 23% (with constant 7% Mo) did not significantly affect the catalyst surface area (decrease from 7.4 to 7.1 m^2g^{-1} for catalyst 6). That is contrary to what Nagai et al. [15] report, which is that for Ni-Mo catalysts increasing Ni loading decreases the catalyst surface area. However, they tested unsupported catalysts with lower Ni content than used in this work. In contrast, increasing the amount of Mo by 50%, with constant Ni loading for Ni-Mo/YSZ supported precursors, increased the surface area from around 6.2 m^2g^{-1} (for 13Ni-**3.5Mo**/YSZ - catalyst 7) to 7.4 (for 13Ni-**7Mo**/YSZ - catalyst 1). However, further addition of Mo, with unchanged 13%Ni content, reduced the area by about 20% up to 5.8 m^2g^{-1} for 13Ni-**16Mo**/YSZ (catalyst 8). This can be attributed to blocking pores of support or formation of bigger particles (Mo-rich phase). Usually, a nominal loading of the added metal element above 20% can result in a decrease in catalyst surface area by blocking support porosity. This suggests that catalyst surface area strongly depends on the Ni:Mo proportions.

According to the Ni-Mo binary phase diagram [16], there are three known compounds at operation temperature 750°C depending on Ni-Mo proportion: Ni_4Mo (catalysts 6 and 7), Ni_3Mo (catalysts 1-5) and NiMo (catalyst 8). Additionally, the ionic radii of Ni and Mo are close; therefore, some solubility is expected because solvent and solute atoms are similar in atomic size. But, the formation of the Ni-Mo solid solution slightly expanded the Ni lattice because of the slightly larger Mo atoms. The obtained catalysts 1 to 5 and 8 have Mo concentrations above the limit for Mo solubility (27%) in metallic Ni-Mo solid solution [16]. Additionally, the crystal structure of Ni and Mo is different **(Mo body-centred cubic, Ni cubic close-packed) with different** lattice parameters. Therefore, depending on the Ni:Mo molar ratio, it is possible to prepare compounds that might have novel catalytic properties.

Catalytic evaluation - oxide catalyst precursors

The reducibility of prepared catalysts was analysed by thermogravimetry (TG and DTG curves in H_2 flow) of 13Ni-7Mo catalyst precursors supported by YSZ (Fig. 1a), GDC (Fig. 1b), Al_2O_3 (Fig. 1c), TiO_2 (Fig. 1d), and CSZ (Fig. 1e).

Tested support materials were stable at the tested temperature and reducing atmosphere. Only the GDC and CSZ support showed a small mass decrease (0.8% and 0.4% respectively) at the temperature above 500°C probably related to cerium reduction. The DTG curves of all the Ni-Mo/supported catalyst precursors showed two endothermic peaks during reduction. Both observed mass-reduction peaks are attributed to the reduction of Ni-Mo oxides. The first reduction peak is attributed to the reduction of oxides NiO and MoO_3 (either bulk and/or nanoparticles), which have a weak interaction with the support. The second peak is attributed to oxides that interact strongly with the support and/or big bulk particles. The peaks related to release of H_2O and decomposition of hydroxides were not present since all tested catalysts were annealed before the reduction process.

The DTG curve showed a strong endothermic peak at 539°C and a weak endothermic peak at 732°C for the Al_2O_3 supported catalyst (Fig. 1c). The curves of the **GDC and CSZ** supported catalyst precursors (Fig. 1b and 1e) were similar to the 13Ni-7Mo/**Al_2O_3** precursor. However, for the **YSZ** supported catalyst the maximum reduction temperature for both peaks was lower with 508°C for the first intensive peak and 668°C for the second peak (Fig. 1a). This suggests lower interaction with **YSZ** support. The reduction temperature observed was more than 80°C higher than the temperature reported in literature for unsupported Ni-Mo precipitates [4]. Interaction with the support increased the reduction temperature and at the same time increased resistance to sintering. The DTG curve of the 13Ni-7Mo/**TiO_2** catalyst precursor was different. The intensity of the endothermic peak at 650°C was higher than that at 479°C, with weight losses of 1.9% and

2.7%, respectively (Fig. 1d). The TiO_2 supported catalyst required higher reduction temperature, suggesting the formation of bigger particles more difficult to reduce ; which was confirmed by the decrease in the BET surface area after Ni-Mo loading. For the Ni-Mo/**GDC,** the second endothermic peak was at 669°C; however, above that temperature, the catalyst mass decreased by 0.9%, indicating poor thermal stability. The tested catalysts with cerium in the support structure were unstable in the reducing atmosphere. Only a small amount of CeO_2 can be reduced at the tested reaction conditions [17]. TPR results showed that the presence of metals Ni-Mo enhanced the ceria reducibility. However, the partially reduced ceria can improve catalyst coke resistance [18].

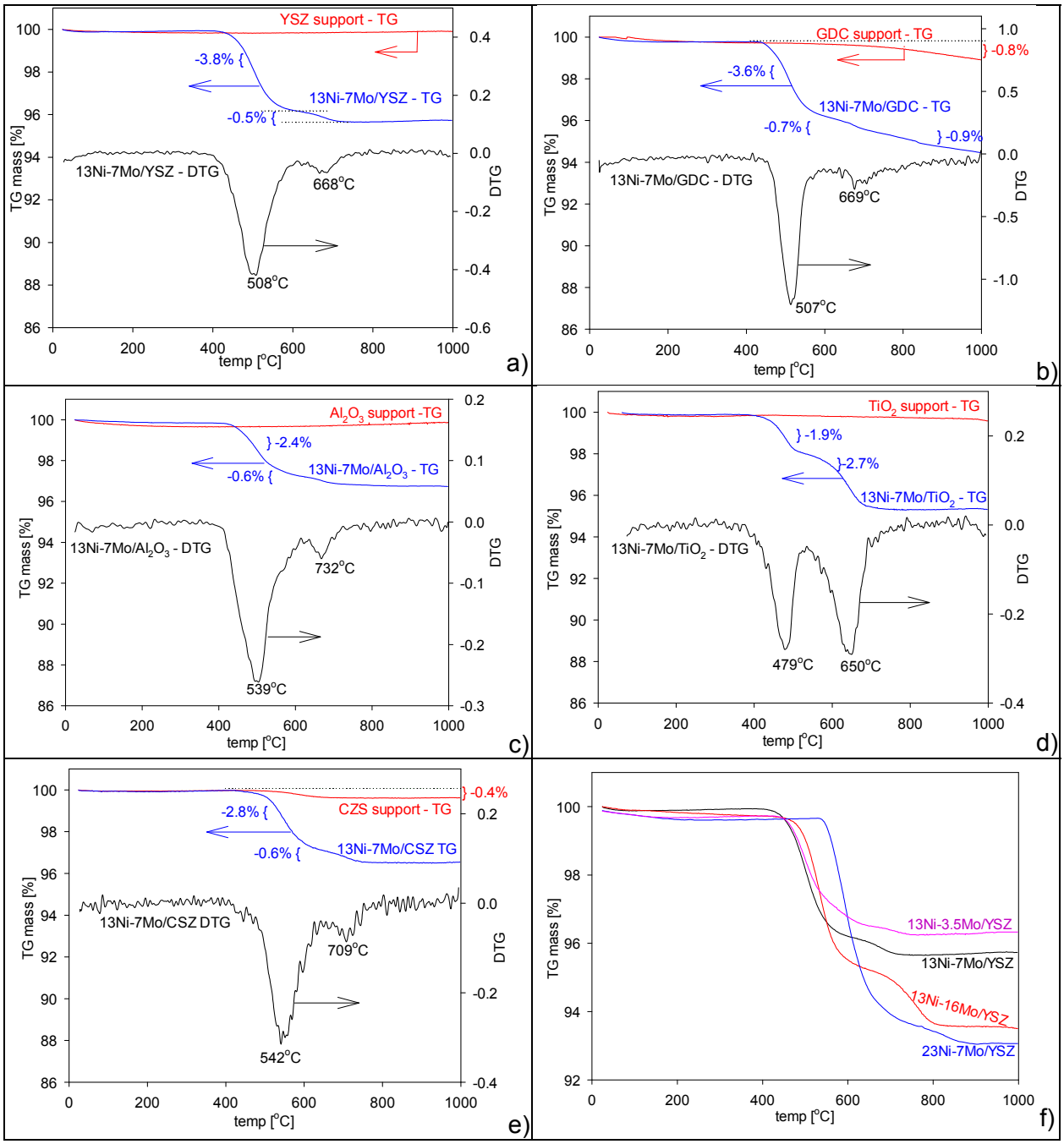

Fig. 1. TG and DTG curves of 13Ni-7Mo catalyst precursors; supported by: a) YSZ, b) GDC, c) Al_2O_3 and d) TiO_2, e) CSZ. f) TG curves of YSZ supported catalysts – various Ni-Mo compositions.

Fig. 1f presents results from the reduction of YSZ supported catalysts with various Ni-Mo compositions. Modification to Ni:Mo loading changed the reduction behaviour. Increasing the loading of Mo increased the mass change during reduction owing to the higher metal oxide loading (Fig. 1f Mo: 3.5, 7 and 16%). Increasing Mo loading from 3.5 to 7% changed the mass reduction at around 450°C bud did not affect the TGA at 650°C and above.
The observed increase of the BET surface area suggests the formation of small particles. Increasing Mo loading to 16% significantly affected reduction at 650°C increasing the mass change. That suggests the formation of bulk Mo-Ni structures difficult to reduce; confirmed by the decrease in the BET surface area. It can be concluded that co-deposition of Mo affected the interaction of Ni-Mo species with YSZ support; that can be attributed to the integration of Ni and Mo and formation of alloys. Increasing amount of Ni from 13 to 23% increased the reduction temperature by around 50°C. The increase in reduction temperature after the increase in Mo or Ni loading can suggest bulk effects and formation of a solid solution with enhanced interaction with the surface. The decrease in the BET surface area suggested pore blocking and formation of larger Ni-Mo particles
The mass reduction of catalysts (13Ni-7Mo) during reduction was caused by the reduction of Ni-Mo oxides. However, the change of mass observed during the reduction process was smaller than expected for the used amount of Ni and Mo loading. This suggests that not all Ni and Mo were in the form of oxides after catalyst sintering. The co-deposition followed by annealing resulted in the formation of Ni-Mo alloy structures deposited on the YSZ surface. The conclusions from TPR analyses were further enhanced by XRD patterns of as-prepared and reduced catalysts. The crystal structure of prepared catalysts changes significantly during reduction. XRD characterisation of the sample oxide precursor of the Ni-Mo/Al_2O_3 catalyst disclosed two groups of peaks (Fig. 2a). One group corresponds to the Al_2O_3 support (marked by squares) while another group can be indexed to the Ni-Mo oxides (all the peaks circled - Fig. 2a). All peaks circled blue for the as-prepared sample (Fig. 2b) can be attributed to $NiMoO_4$ and other oxide Ni-Mo forms formed during passivation. As is shown in the XRD pattern, after reduction/carburisation, all diffractogramme peaks related to the support remained unchanged with identical intensity (Fig. 2b). However, all diffraction peaks related to Ni-Mo oxides disappeared and new peaks appeared related to Ni-Mo metal and Mo-C structures. This confirms completed reduction to the metallic form for Ni and Mo. A similar effect was observed for all tested catalysts. The completed reduction should prevent coke deposition. It was reported [14] that for Ni-Mo catalysts incomplete reduction/carburisation can lead to an increase in coke deposition during reforming.

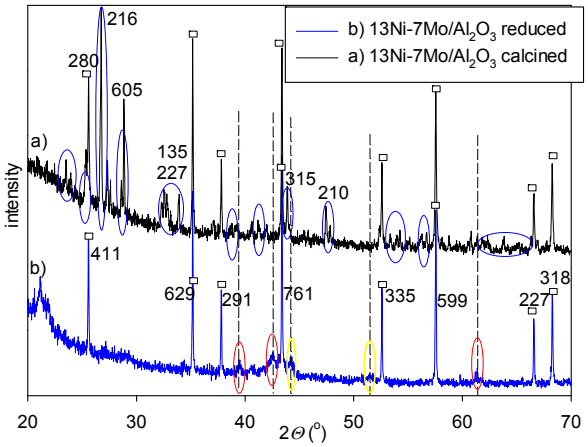

Fig. 2. XRD diffractograms of 13Ni-16Mo/Al_2O_3 catalyst: a) after calcination b) reduced.

Physicochemical characterisations - reduced catalysts

The Ni-Mo catalyst precursors synthesised by chemical precipitation were characterised by XRD. Intensive peaks related to support material were marked respectively: (□) Al_2O_3, (■) GdO_3 (or GdO and CeO_2), (○)TiO_2, (●) MoO_2 (Fig. 3). Compared to the sharp well-resolved peaks corresponding to support materials, all peaks related to Mo-Ni crystallites were broad and much less intensive indicating the low crystallinity of the Ni and Mo phase for all tested catalysts. The formation of broad diffraction peaks may suggest the formation of a solid solution. The small peaks at 2Θ 44.4, 51.8° are specific to metallic Ni. The peaks observed at 2Θ 44.4 were weak and wide and could be associated to Ni-Mo intermetallic/alloy compounds (NiMo, Ni_4Mo, Ni_3Mo, Ni_3Mo_3C and/or MoC), however, it cannot be excluded that these may be related to carbon deposition during preparation. Carbon can sometimes deposit on the molybdenum carbide during carburisation [11]. The most intensive monometallic Ni related peak at 2Θ 51.8° was observed for the GDC support. No evidence of monometallic Mo phase or molybdenum oxides was observed after catalyst reduction implying a possible absence of Mo bulk crystal particles.

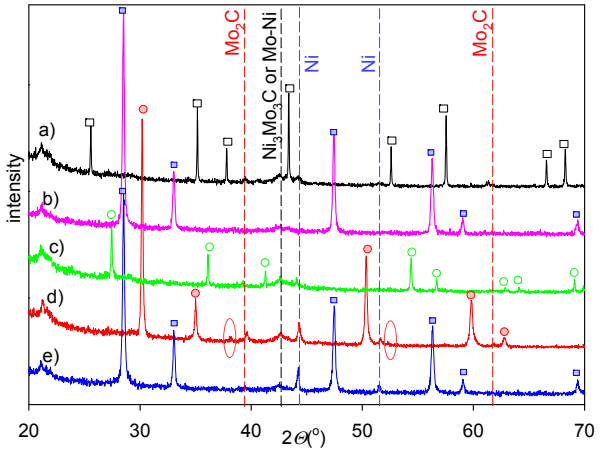

Fig. 3. XRD diffractograms of the 13Ni-7Mo catalysts supported by: a) Al_2O_3, b) CSZ, c) TiO_2, d) YSZ, e) GDC.

The dissolution of the Mo phase into the Ni lattice and alloy formation can affect the lattice distortion and formation of the mixture of NiMo, Ni_4Mo, Ni_3Mo intermetallic phase [6]. Only residual carbide levels were observed by X-ray diffraction (XRD) after the synthesis. Molybdenum carbides have four crystal structures (α-MoC_{1-x}, β-Mo_2C, γ-MoC, η-Mo_3C_2. The intensity of the obtained XRD diffractograms did not allow to unambiguously distinguish the obtained carbide form (caused by low Mo concentration and overlapping by the high-intensity signal from the support material). But they suggest that the selected synthesis conditions lead mostly to the formation of β-Mo_2C. Diffraction peaks related to MoC were not detected. A highly amorphous and low intensive phase attributed to Mo_2C with the characteristic XRD peak at 2Θ 39.8 was detected for all reduced Ni-Mo supported catalysts except GDC (were more intensive for Al_2O_3 and YSZ supported catalysts). Additionally, for Al_2O_3 and YSZ supported catalysts, a peak was detected at 2Θ 61.9° that could be attributed to the presence of Mo_2C. Additionally, for the YSZ supported catalyst, small peaks were detected at 2Θ 34.8° and 52.5°, that could also be attributed to the presence of Mo_2C. If those two peaks were also present for the Al_2O_3 supported catalyst, they were overlapped by intensive peaks from the support material.

The results obtained suggest that YSZ and Al_2O_3 promote the formation of a Mo phase that is converted to Mo_2C during reduction/carburisation. Mo_2C in known to promote H_2 production [11]. The low intensity of Ni related peaks suggested the formation of

amorphous Ni structures, especially for the TiO_2 and CSZ supported catalysts. Peaks attributed to the Ni phase had a higher intensity for the GDC and YSZ supported catalysts, indicating higher crystallinity of the Ni probably related to the formation of more agglomerated Ni-rich nanoparticles. The lack (or small concentration below XRD detection) of Mo_2C on TiO_2, GDC or CSZ supported catalysts suggested high molybdenum oxide dispersion and strong interaction with the support which makes it more difficult to convert to carbide.

YSZ supported Ni-Mo catalysts

From the tested Mo-Ni catalysts, the most promising for application in internal SOFC reforming appeared to be the YSZ supported catalyst. Therefore, this catalyst was further investigated. The aspect that was studied in more detail was the influence of Mo and Ni loading. According to literature [14], an increase in Ni:Mo ratio can enhance conversion of less active Mo-C structures into more active Mo_2C. With the increase in Mo concentration to 16% (and constant Ni 13%), the intensity of Mo_2C peaks slightly decreased and simultaneously diffraction peaks related to Ni became less intensive (Fig. 4a). Low intensity of Mo_2C peaks even at 16% Mo loading suggested a low Mo_2C ratio to total Mo species in the prepared catalysts. Peaks for MoO_2 were not detected. From XRD diffractograms for higher Ni loading (Fig. 4b - 23%Ni-7%Mo), it was observed that the intensity of Ni metal related diffraction peaks increased with increasing in Ni loading. That suggests the formation of a Ni-rich phase. However, it slightly reduced the intensity of Mo_2C related peaks (compared to 13%Ni-7%Mo - Fig. 4c). This observation suggests that there is an optimum Ni:Mo ratio (close to 13%Ni-7%Mo) that promotes the Mo carburisation process for the YSZ supported catalyst. It can be seen that Mo_2C as a catalyst requires doping of additional metal. Increasing Ni loading above 13% or changing the 7% Mo loading, both reduced Mo carburisation.

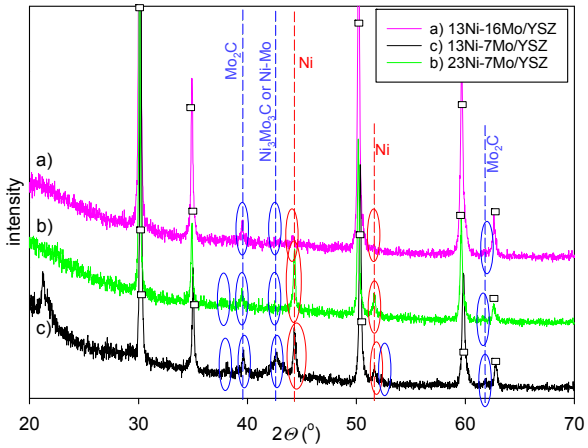

Fig. 4. XRD diffractograms of the Ni-Mo YSZ supported catalysts a) 13%Ni-16%Mo, b) 13%N-7%Mo, c) 23%Ni-7%Mo.

The material morphology was characterised by the SEM images of the synthesised Ni-Mo/YSZ catalyst. The catalyst precursor (Fig. 5A-B) exhibited various morphologies compared to the catalyst after heat treatment and reduction Fig. 5C-D). After deposition, the Ni-Mo was distributed on the YSZ structure in a mix of grains and flake-like shaped particles distributed on the support. The calcination followed by reduction/carburisation resulted in the formation of grains/crystals equally distributed on the YSZ surface. YSZ particles display disorderly stacked, irregular shape particles in the size range of 0.5 to 2 µm, while Ni-Mo particles (on the YSZ surface) were spherical and 5 to 20 nm in size. The

small size of the Ni-Mo particles could affect the XRD analyses and could be one of the reasons for the low intensity of the Ni-Mo diffraction peaks. The observed formation of Ni-Mo nanospheres was a promising tendency for the formation of good coke resistance and stable catalysts that can support internal SOFC reforming. The proven high dispersion of the catalyst allowed exposing active sites and confirmed the possibilities for the application of deposition-co-precipitation as a method to control the catalyst morphology under SOFC operation. The obtained high dispersion maximised the exposition of active sites.

TEM analyses were conducted to further investigate the catalyst morphology. Typical TEM micrographs of the reduced Ni-Mo/YSZ catalysts, presented in Fig. 6, supported the observation of formation of bimetallic Ni-Mo alloy nanospheres. Figs. 6A-B show that Ni-Mo nanoparticles are homogeneously dispersed on the YSZ support. Fig. 6B shows the periodically visible sets of lattice fringes for Ni-Mo phase. The high-resolution TEM revealed a petal-like structure of Ni-Mo nanocrystals. The lattice spacing was 0.8 to 1.1 nm size. The EDS measurement confirmed that those small grains of 5 to 20 nm visible on the surface of bigger particles (Fig. 6) were Ni-Mo binary particles.

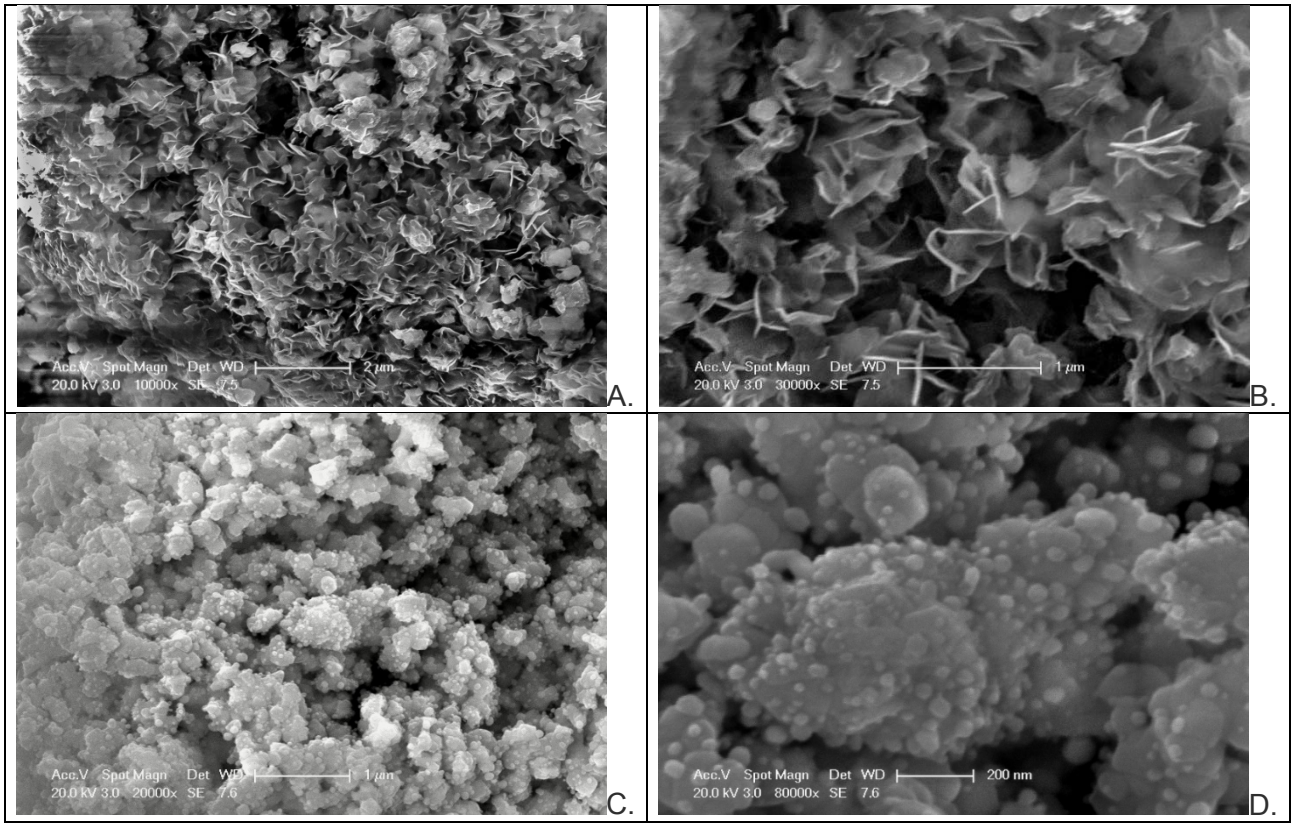

Fig. 5. SEM images (various magnification) of 23%Ni-7%Mo/YSZ powder prepared using the deposition-co-precipitation method. A-B after deposition C-D reduced.

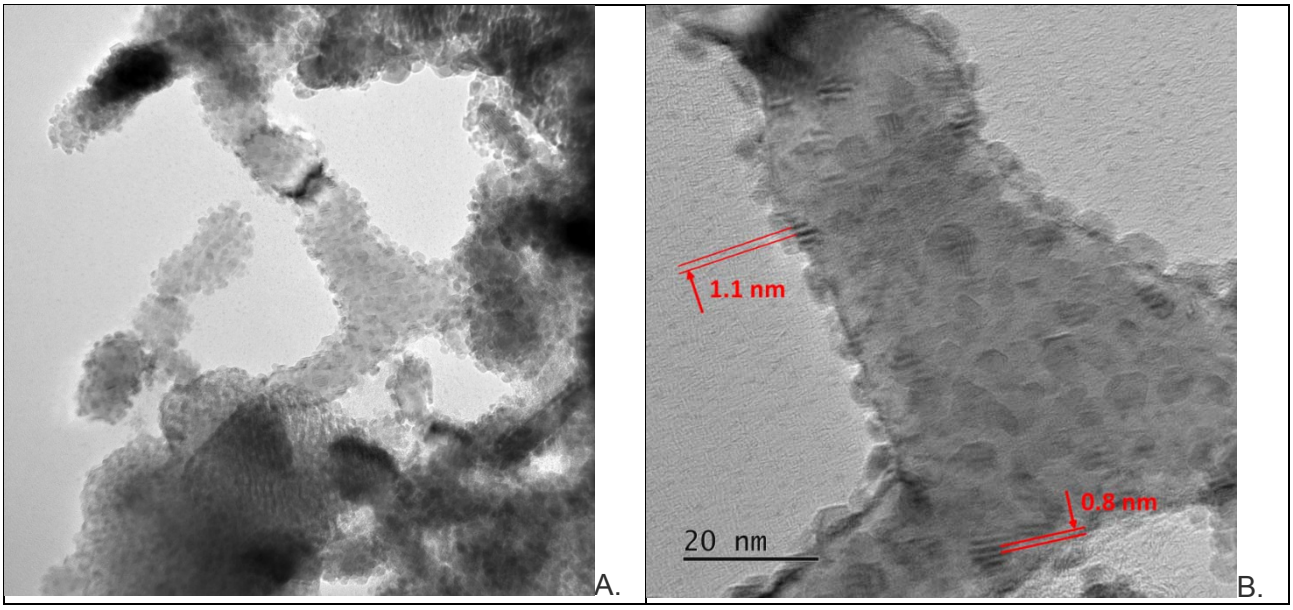

Fig. 6. TEM images (various magnifications) of 23Ni-7Mo/YSZ reduced powder prepared using the deposition-co-precipitation method.

Composition measurements underestimated the amount of segregation at a boundary caused by beam broadening due to the magnification used. Measurements that concentrated on areas with high concentration of visible small crystal structures confirmed the concentration of Ni and Mo. When EDS measurements were taken on areas of support with the absence of those grains, they showed the absence of those elements. This suggests that most Ni and Mo are deposited as nanograins after the catalyst reduction. The micrographs also show that Ni-Mo particles have near-spherical shape well dispersed on the support surface. Unsupported Ni-Mo nanoparticles were not observed.
On SEM (Fig. 5) and TEM (Fig. 6) scans of the reduced catalyst, coke deposition was not detected. It was reported [7] that for some Mo catalysts the carburisation step can result in coke formation which deactivates the catalyst.

3. Summary

Supported Ni-Mo catalysts were synthesised using the deposition-co-precipitation method. The variation of supports and molar ratio of the Ni:Mo led to various morphologies, reduction temperatures, and reforming activities. The optimum Ni:Mo ratio that promoted the Mo carburisation process for the YSZ supported catalyst was close to 13%Ni:7%Mo. Reduced Ni-Mo catalysts showed the typical XRD peaks of Ni amorphous phases and MoC_2 was detected on the Ni-Mo catalysts supported by YSZ and Al_2O_3.
This preparation method could result in the formation of more effective cheaper SOFC anodes, however, there are still many parameters requiring consideration in order to understand the process alongside with SOFC experiments. Prepared Ni-Mo catalysts supported by YSZ, GDC and CSZ with improved carbon tolerance have the potential to be used as anodes in SOFC. Those catalysts were compared to catalysts typical for reforming supports Al_2O_3 and TiO_2. Further investigation is currently under way in the process to evaluate properties of the described materials and their application as SOFC anodes.
Results from the evaluation of synthesised catalysts under various conditions will be submitted as a separate publication.

Acknowledgements
The results are part of the outcome of the "Biogas to energy - catalyst for biogas combined steam/dry reforming" project funded under EPSRC/University of Birmingham Global Challenges Research Fund: 1516GCRF018 and EPSRC JUICED Hub EP/R023662/1.

References

1. Asset, T., et al., *Highly active and selective nickel molybdenum catalysts for direct hydrazine fuel cell.* Electrochim. Acta, 2016. **215**: p. 420-426.
2. Fang, M., et al., *Hierarchical NiMo-based 3D electrocatalysts for highly-efficient hydrogen evolution in alkaline conditions.* Nano Energy, 2016. **27**: p. 247-254.
3. Liu, H., et al., *Synthesis, characterization and hydrodesulfurization properties of nickel–copper–molybdenum catalysts for the production of ultra-low sulfur diesel.* Fuel, 2014. **129**: p. 138-146.
4. Liu, H., et al., *Preparation of highly active unsupported nickel–zinc–molybdenum catalysts for the hydrodesulfurization of dibenzothiophene.* Appl. Catal. B, 2015. **174–175**: p. 264-276.
5. McKone, J.R., et al., *Ni–Mo Nanopowders for Efficient Electrochemical Hydrogen Evolution.* ACS Catal., 2013. **3**(2): p. 166-169.
6. Hua, B., et al., *Facile Synthesis of Highly Active and Robust Ni–Mo Bimetallic Electrocatalyst for Hydrocarbon Oxidation in Solid Oxide Fuel Cells.* ACS Energy Lett., 2016. **1**(1): p. 225-230.
7. Ma, Y., et al., *Catalytic Activity and Stability of Nickel-Modified Molybdenum Carbide Catalysts for Steam Reforming of Methanol.* J. Phys. Chem., 2014. **118**(18): p. 9485-9496.
8. Troskialina, L., A. Dhir, and R. Steinberger-Wilckens, *Improved Performance and Durability of Anode Supported SOFC Operating on Biogas.* ECS Trans., 2015. **68**(1): p. 2503-2513.
9. McIntosh, S., J.M. Vohs, and R.J. Gorte, *Effect of Precious-Metal Dopants on SOFC Anodes for Direct Utilization of Hydrocarbons.* Electrochem. Solid-State Lett., 2003. **6**(11): p. A240-A243.
10. Majewski, A.J., J. Wood, and W. Bujalski, *Nickel–silica core@shell catalyst for methane reforming.* International J. Hydrogen Energy, 2013. **38**(34): p. 14531-14541.
11. Ma, Y., et al., *Molybdenum carbide as alternative catalyst for hydrogen production – A review.* Renewable Sustainable Energy Rev., 2017. **75**: p. 1101-1129.
12. Shi, C., et al., *Ni-modified Mo2C catalysts for methane dry reforming.* Appl. Catal. A, 2012. **431-432**: p. 164-170.
13. Lin, S.S.Y., et al., *Steam reforming of methanol using supported Mo2C catalysts.* Appl. Catal. A, 2007. **318**: p. 121-127.
14. Hirose, T., Y. Ozawa, and M. Nagai, *Preparation of a Nickel Molybdenum Carbide Catalyst and Its Activity in the Dry Reforming of Methane.* Chin. J. Catal., 2011. **32**(5): p. 771-776.
15. Nagai, M., A.M. Zahidul, and K. Matsuda, *Nano-structured nickel–molybdenum carbide catalyst for low-temperature water-gas shift reaction.* Appl. Catal. A, 2006. **313**(2): p. 137-145.
16. Wang, Y., et al., *Structural stability of Ni–Mo compounds from first-principles calculations.* Scr. Mater., 2005. **52**(1): p. 17-20.

17. Kundakovic, L. and M. Flytzani-Stephanopoulos, *Cu- and Ag-Modified Cerium Oxide Catalysts for Methane Oxidation.* J. Catal., 1998. **179**(1): p. 203-221.
18. Papaefthimiou, V., et al., *On the Active Surface State of Nickel-Ceria Solid Oxide Fuel Cell Anodes During Methane Electrooxidation.* Adv. Energy Mater., 2013. **3**(6): p. 762-769.